Intermetallics 131 (2021) 107106

Contents lists available at ScienceDirect

Intermetallics

journal homepage: http://www.elsevier.com/locate/intermet

# Low energy atomic traps sluggardize the diffusion in compositionally complex refractory alloys

Ankit Roy, Joydeep Munshi, Ganesh Balasubramanian *

*Department of Mechanical Engineering and Mechanics, Lehigh University, Bethlehem, PA, USA*

ARTICLE INFO

*Keywords:*
Compositionally complex alloys
Diffusion coefficient
Molecular dynamics
First-principles
Creep resistance
Low energy atomic traps

ABSTRACT

Compositionally complex alloys (CCAs) have attracted significant attention over the past decade due to their potential for exhibiting excellent mechanical properties even at elevated temperatures. The resistance to creep deformation at temperatures greater than one-half of the melting point is primarily driven by atomic diffusion, but experimental measurement of the diffusion coefficients at elevated temperatures is challenging due to the instrumentation limitations and possible oxidation of the alloy. We employ molecular dynamics simulations and first-principles calculations to examine the atomic diffusion of the various elemental species in a refractory CCA containing Mo-Ta-Ti-W-Zr as the constituents. The predictions reveal that diffusion coefficients in CCAs are slower than the corresponding diffusion in the pure metals by a factor of ~8–12, while the activation energies for the diffusion are relatively much higher. A strong attraction between unlike atomic pairs in the CCA coupled with the occurrences of low energy atomic traps due to preferential site-occupancy of the elements creates an ~1 eV energy barrier that significantly impedes atom migration. The sluggish diffusion reduces the creep deformation strain rates, increasing the resistance to creep for the CCA at high temperatures.

## 1. Introduction

Compositionally complex (multicomponent) alloys (CCAs), have received widespread attention over the last decade [1,2]. This growth in interest is partly attributed to the relatively high entropy of mixing that stabilizes the solid-solution phase and prevents the formation of intermetallic compounds [3], whence the intriguing microstructural phase formation and structural properties emerge. Certain CCAs have exhibited excellent high temperature mechanical strength [4,5], hardness [6], stiffness [7], wear and corrosion resistances [8,9]. Hsu et al. [10] defined a softening transition temperature ($T_T$) for these alloys, where a change in the deformation mechanism reduces the hardness of CCAs above the $T_T$. While dislocation glide is the predominant creep deformation mechanism below the softening transition temperature (typically $\geq 0.5\ T_m$ [5], where $T_m$ is the absolute melting temperature) of such concentrated solid-solutions, for higher temperatures, creep occurs by diffusional flow of the atoms [10]. Diffusion in solids, primarily driven by the presence of atomic defects, is 2-3 orders of magnitude slower (*i.e.,* sluggish) than in liquids. Thus, in effect, the creep resistance above $T_T$ depends on the ability of the different atomic species to migrate to a neighboring vacancy.

Sluggish diffusion [11,12] has been cited, albeit with certain aberrations, as one of the four key factors for the novel material properties of CCAs [13–16]. The liquid phase properties are important in that they can potentially provide insights into the nucleation and crystal growth processes [17], as well as growth kinetics and dendritic arm spacing in microstructures during solidification [18]. Note that these multicomponent alloys differ from their conventional counterparts in that no distinct solvent or solute species can be specified. Consequently, due to the presence of multiple species in the matrix, the enthalpies required for vacancy formation and atomic migration from one lattice site to another can significantly differ for each element [19]. These fluctuations create variations in the lattice potential energy (LPE) across the atomic sites, such that the sites with lower LPE act as atomic blocks with high activation energies, and impede atom migration [20]. Here, we investigate the effect of alloy composition on atomic diffusion, and offer a fundamental understanding of the physics underlying the (sluggish) diffusion especially at elevated temperatures. We employ classical molecular simulations and first-principles calculations to model the diffusion mechanism in a non-equiatomic CCA, *viz.*, $(Mo_{0.95}W_{0.05})_{0.85}Ta_{0.10}(TiZr)_{0.05}$ alloy that exhibits excellent tensile and compressive strength [21]. The results, as elaborated below, reveal that

* Corresponding author. Packard Laboratory 561, 19 Memorial Drive West, Bethlehem, PA, 18015, USA.
*E-mail address:* bganesh@lehigh.edu (G. Balasubramanian).

https://doi.org/10.1016/j.intermet.2021.107106
Received 16 July 2020; Received in revised form 26 December 2020; Accepted 12 January 2021

the diffusion coefficient [22] near $T_m$ for these alloys is lower than that in the corresponding pure metals because the formation of low energy atomic traps in the alloy lattices increases the energy required for the atom to migrate to a vacancy.

## 2. Computer simulation methods

Molecular dynamics (MD) simulations are employed using the extensively parallelized Large-scale Atomic/Molecular Massively Parallel Simulator (LAMMPS) package [23], while VESTA [24] and OVITO [25] are used for visualization and data-processing. A cuboidal simulation box is constructed with Mo, Ta, Ti, W and Zr atoms distributed randomly in a BCC lattice of $(31.5a \times 31.5a \times 31.5a)$ $nm^3$ dimensions, where $a = 0.317$ *nm* is the lattice constant [21]. Periodic boundaries are imposed along all three directions. The atomic interactions are described using the EAM potential [26]. We use the parameter combinatorial tool built within the LAMMPS package [26] to obtain a hybrid potential encompassing the 10 cross interactions between all the elements and construct a collective forcefield for the Mo-Ta-Ti-W-Zr alloy system. Such a technique has been previously validated to successfully simulate the crystallographic phase and stress strain curves for the $(Mo_{0.95}W_{0.05})_{0.85}Ta_{0.10}(TiZr)_{0.05}$ [21] and $Al_{10}CrCoFeNi$ [27] alloys. Additionally, the BCC phase and elastic modulus of the Mo-Ta-Ti-W-Zr alloy system obtained from MD simulations were experimentally validated [21]. The alloy lattice is energy minimized by the conjugate gradient method with an energy tolerance of $10^{-15}$ eV and a force tolerance of $10^{-15}$ eV/Å. The alloy is initiated at 3300 K under the isothermal-isobaric (NPT) ensemble for 300 ps at 0 MPa pressure and then rapidly quenched to 1100 K with a constant quenching rate of 200 K/ns. The equilibrated structure, shown in Fig. 1(a), is principally a single-phase BCC solid-solution. To calculate the diffusion coefficients ($D$) of each element, atomic positions and velocities are recorded at 3300 K, 2800 K, 2100 K and 1900 K for every 200 ps [28], after equilibrating for 300 ps at each temperature similar to prior reports [21,28]. $D$ is obtained from the slope of the linear mean square displacement (MSD) [29] as

$$D = \frac{1}{6}\partial\left(\frac{1}{N}\sum_{i=1}^{N}\left(x_i(t) - x_i(0)\right)^2\right) \Big/ \partial t \tag{1}$$

Here, $N$ is the total number of atoms in the melt, and $x_i(t)$ is the location of ith atom at time $t$. Additionally, we calculate the structural pair correlation function $g_{\alpha\text{-}\beta}(r)$ that reveals the coordination tendencies between like or unlike pairs of atoms in the alloy. $g_{\alpha\text{-}\beta}(r)$ provides the probability of the presence of another atom at a distance $r$ from the atom under consideration [30], and its integral provides the number of nearest neighbors within a range $r$ of that atom.

We compute the mean difference in the energies of the CCA crystal lattice before and after an atom migrates to a vacancy using density functional theory (DFT) calculations with the Vienna *ab initio* simulation package (VASP) [31]. The system is initiated as a solid solution with a BCC crystal and each metal has at least one atom occupying one body center lattice site and at least one atom occupying the corner site. The configuration employed for the first-principles calculations contains 16 atoms in a periodic box. The chosen simulation suffices our purpose to interrogate the difference in energy within the alloy lattice arising from the migration of an atom to a vacancy site. Previous reports [32] have simulated systems of similar sizes to calculate vacancy formation enthalpies in a 4 component FeCoCrNi CCA. Projector-augmented-wave (PAW) potential with Perdew-Burke-Ernzerhof (PBE) scheme is employed and generalized-gradient approximation (GGA) is used for the exchange correlation calculations [33–35]. For diffusion to initiate, the activation energy barrier needs to be overcome to displace an atom from its initial position to the vacancy. In a symmetrical environment (*i.e.*, same metal atom at every lattice site), the minimum energy before and after the atom displacement are equal as in the case of pure metals [19]; but in an asymmetrical environment (*i.e.*, different metal atom at each lattice site), the minimum energy before and after atom displacement does not assume the same magnitude. There is a finite difference between the two energy levels that equals the mean difference in energy as in the case of CCAs [20]. To simulate and calculate the mean energy difference $E^x_{MD}$ of the system for an atom of a certain metal to migrate to a vacancy, the processes illustrated in Fig. 1(b) and (c) are employed. One atom of that certain element is deleted at a time from the corner position A of the cubic lattice, and the system is allowed to relax completely, thus creating an initial vacant position at this site A. Next, another atom of same metal is deleted from the body center position B of the cell and the system is allowed to relax completely. This step connotes that the atom from cube center has migrated to the cube corner. $E^x_{MD}$ is denoted as the difference in energy of the structures between the states when an atom of the metal $x$ is missing from position A, and then position B.

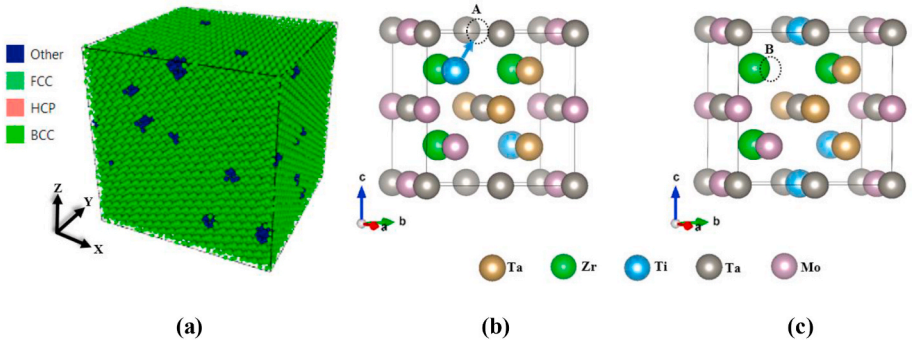


**Fig. 1. (a)** Analyses of the structural coordination for the equilibrated $(Mo_{0.95}W_{0.05})_{0.85}Ta_{0.10}(TiZr)_{0.05}$ CCA performed with the common neighbor approach reveals that 96.4% of the simulated alloy structure assumes a BCC lattice configuration, consistent with the literature [21]. This result verifies the choice and accuracy of the potentials used for the MD simulations. **(b), (c)** The methodology to compute the mean energy difference ($E^x_{md}$) of the alloy before and after a Ti atom migrates to a vacant site is illustrated. Site A is an initially available vacancy. The solid arrow indicates the direction in which the Ti atom migrates. $E^x_{md}$ is calculated as the difference in energy of the alloy structures before and after the migration of the Ti atom from position B to A. In a structure consisting of only pure Ti atoms, this difference in energy is nil, but in case of the CCA, $E^x_{md}$ = 1.54 eV (the lattice potential energy with Ti atom at site A = 158.95 eV and at site B = 157.41 eV). This prediction corroborates that in presence of multiple metal atoms in a lattice, there exist low energy atomic traps that hinder atom displacement from that location, contributing in a 1-2 orders of magnitude lower diffusion coefficients in CCAs as compared to pure metals or conventional alloys.

## 3. Results and discussion

In order to identify the melting temperature ($T_m$) an approach previously described in the literature [36] is adopted. Fig. 2(a) reproduces the change in volume of the simulation cell with temperature as the alloy is quenched from 3300 K to 1100 K at a cooling rate of 200 K/ns. Only a limited interval of the temperatures is presented to clearly depict the transition zone. A sharp decrease in volume is noted at ~2114 K that is considered as the theoretical crystallization temperature for the $(Mo_{0.95}W_{0.05})_{0.85}Ta_{0.10}(TiZr)_{0.05}$ CCA. The absence of experimental measurement to validate this temperature prediction is acknowledged. Nevertheless, we utilize spatial correlation functions to derive additional information on the alloy microstructures at temperatures above and below the hypothesized $T_m$. Fig. 2(b) displays the radial distribution function (RDF) of the alloy at 2300 K and at 1900 K from 0 to ~ 7 Å (the cutoff in the EAM potential is 7.15537 Å). The RDF plot excludes the volume of the atoms for about 2 Å, and is thus zero or near zero between 0 and ~2 Å. While experimental results from X-ray or neutron diffraction data to potentially validate the simulation predictions for this CCA is unavailable in the literature, our RDF results at 1900 K reveal similarity in the profile with experimental characterization of a different refractory CCA HfNbTaTiZr (Fig. 2 in Ref. [37]) between 0 and 7 Å. The broadening of the function beyond the first peak at 2300 K (dashed line) reflects a typical signature of liquid behavior [30]. On the other hand, at 1900 K (solid line), the RDF evolution reveals the existence of distinct peaks and hence, the presence of well-defined nearest neighbor shells surrounding an atom displaying long-range order [38]. As reported in the literature [39], we find the average number of atoms in the first shell of this BCC crystallographic phase to be 8, followed by 6 in the next shell. Given this observation we assert that 2114 K can indeed be hypothesized as the $T_m$. Hence, we calculate the diffusion coefficients of the CCA at $T = 1900$ K to ensure that the properties obtained are applicable for temperatures well above $T_T$ and account for the entire range of creep temperatures in the deformation mechanism map [40], but lie well below the crystallization temperature, considering the deviation in identifying the $T_m$ from the MD simulations can be up to ~200 K. Since the MSD in eq. (1) relies upon the concept of random walks experienced by atoms in a lattice, the transient evolution of the random walks exercised by a single atom in the lattice produces a pulse and saw tooth type of wave on a $R^2$ profile ($R = \sum_1^n r_k$ is the displacement vector where n is the number of jumps for the random walks) as a function of the 'number of jumps' [30]. But when the $R^2$ is sampled over a large number of trajectories traced by all the atoms present in the simulation cell, the variation approaches steadily towards a straight line with a positive gradient [30]. These random walks of atoms are largely dependent on the intrinsic ability of the elemental species to move from one site to another in a lattice. Several factors decide the extent of these jumps *viz.*, the strength of the interatomic potentials between the atoms, the mass of the elements, the temperature of the system, and the strength of the interatomic cross interactions between the various species. Fig. S1 shows the transient evolution of MSD for all the constituent metallic elements in the $(Mo_{0.95}W_{0.05})_{0.85}Ta_{0.10}(TiZr)_{0.05}$ CCAs. We note that Ti and Zr exhibit relatively higher slope for the MSD with time, and consequently greater extent of the diffusion relative to the other species in the CCA driven by thermodynamic properties *i.e.,* kinetic energy of the system and atomic masses. At any given temperature, the mean kinetic energies of all the species in the alloy are similar. The atomic masses of the elements are in the order Ti < Zr < Mo < Ta < W. Hence, the lighter elements have a higher mobility under the same energy and force field constraints. Accordingly, Ti has a higher MSD slope owing to higher mobility followed by Zr and Mo. Since Ta and W occupy adjacent locations in the periodic table, the difference in their mobilities is not distinguishable via just the MSD.

The MSD for pure metals is also computed using an identical simulation setup with each metal considered separately (the predictions are illustrated in Fig. S2). We note that the MSD of pure metals are obtained at a different set of temperatures than those used for the alloy. For Ta and W, we use 3700 K, 3300 K and 2800 K to obtain the MSD because the melting points of Ta and W are above 3200 K. Our objective is to predict the atomic velocities and positions near the liquid to solid phase transition zone to analyze the diffusion behavior at the near liquid region. Likewise, we choose the temperatures for obtaining the MSD of the other metals but limiting the upper bound well below the respective vaporization temperatures. In addition to calculating the diffusion coefficient for the metals using Eq. (1), we estimate the activation energy ($Q$) from $Q = -2.3R\frac{\Delta(logD)}{\Delta\left(\frac{1}{T}\right)}$, following the procedure described elsewhere [41, 42]. The activation energies are listed in Table S1 as supplementary information. There is strong agreement between the predictions and prior literature data for Ti and Zr. However, for the other metals deviations between the experimental and computational results are noted that we attribute to differences in the temperatures at which the measurements are performed, and the choice of the interatomic potentials. These diffusion coefficients obtained from MSD data are used to compare the diffusion for the metals in the pure state against that in CCAs, similar to a previous report [20] that had experimentally measured diffusion in Co-Cr-Fe-Mn-Ni alloy and compared them with the diffusion in the constituent metals in the pure state. To prove that diffusion is slower in CCAs, we define an empirical parameter *i.e.,* normalized activation energy, calculated as the ratio of activation energy to the melting temperature. This normalized activation energy is found to be one order of magnitude higher in CCAs than in pure metals, thereby corroborating the retarded diffusion phenomenon in CCAs. Nevertheless, this model has certain drawbacks and characterized as predominantly correlational [22]. It has been reported [22] that in order to compare the diffusion data of pure metals with corresponding

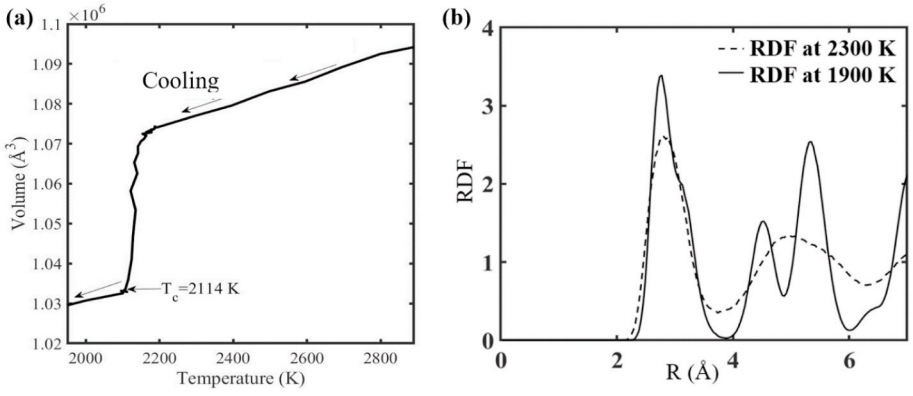


**Fig. 2. (a)** Variation of the average volume of the $(Mo_{0.95}W_{0.05})_{0.85}Ta_{0.10}(TiZr)_{0.05}$ CCA with temperature during cooling at a rate of 200 K/ns. Upon cooling the liquid metal mixture crystallizes into a single-phase BCC solid solution as shown previously in Fig. 1. A crystallization temperature of ~2114 K is identified based on the steep change in the gradient of volume shrinkage. **(b)** RDF of the atoms in $(Mo_{0.95}W_{0.05})_{0.85}Ta_{0.10}(TiZr)_{0.05}$ CCA at 2300 K (dashed line) and 1900 K (solid line) are presented. Note that the evolution of peaks at 1900 K highlights the onset of long-range order thereby evincing the occurrence of crystallization. The absence of well-defined peaks at 2300 K indicates the nonexistence of long-range order thereby corroborating that the existence of liquid phase at 2300 K.

diffusion data in CCAs, a reduced form of diffusion coefficients is rather suitable [43,44]. This proposition arose from the various analyses of the diffusion of, say metal A and metal B in the solid solution AB, where the ratios of vacancy formation energy, self-diffusion energy and chemical diffusion energy with solidus temperature was found to depend only the relative concentrations. Therefore, to effectively compare the diffusion coefficients of metals relative to when they exist within an alloy, an alternate approach has been proposed with a dimensionless diffusion coefficient as [43]:

$$D^* = D_0^* exp\left(-\frac{Q^*}{T^*}\right) \tag{2}$$

Here, $T^* = \frac{T}{T_m}$, $Q^* = \frac{Q}{kT_m}$ with $k$ the Boltzmann constant, $D_0^*$ the dimensionless temperature independent preexponential, $Q$ the activation energy, and $D^* = D\left(\frac{kT_m a^2}{M}\right)^{-0.5}$ with $a$ being the lattice constant and $M$ the atomic mass. We use $T_m = 2114$ K as hypothesized from results of Fig. 2(b) when calculating $D^*$ for the metals in the CCA, while $a$ and $M$ are calculated using Vegard's rule [44]. The variation of $D^*$ with inverse of $T^*$ for the different elements of the CCA in Fig. 3, as anticipated reveals a consistent decrease in the diffusion of the various elements both in the CCA as well as in the pure metallic forms. There is a systematic downward shift in the solid straight lines that represent the alloy compared to the dashed lines that represent the pure metals. The dimensionless diffusion coefficients of the constituent elements in the alloy are smaller than that in pure state by a factor of ~ 8–12. This observation together with higher (~1.1–2.3 × ) activation energies (Table S1) of elements in the alloy corroborate the sluggish diffusion effect. In particular, Ti exhibits the highest increment in activation energy required for diffusing within the CCA although it has the smallest atomic radius and greatest $D$ amongst the constituent elements of the alloy. We attribute this behavior to the strong interatomic interactions (evinced by the strong affinity between unlike atomic pairs as shown by

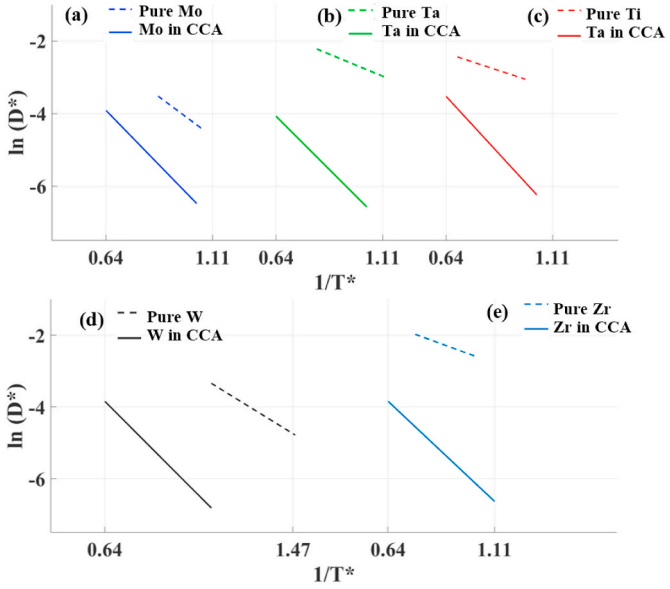


**Fig. 3.** Dimensionless diffusion coefficient ($D^*$) as a function of inverse reduced temperature presented for all constituent metals **(a)** Mo, **(b)** Ta, **(c)** Ti, **(d)** W and **(e)** Zr in the CCA. For all the elements, $D^*$ is higher in their pure metallic form than when present in the CCA by a factor of ~ 8–12. The ratios of activation energies required for the diffusion of each of the elements in the CCA relative to the corresponding pure metals are >1, as noted from Table S1, confirming that higher activation energies are required when in the alloy. This ratio is highest for Ti and together with its lowest atomic mass amongst the constituent elements of this CCA, strongly retards its mobility due to the interatomic interactions in presence multiple atomic species in the alloy.

$g_{\alpha\text{-}\beta}(r)$ in Fig. S3 provided as supplementary information) in the neighborhood of a Ti atom in the concentrated solid solution. The relatively limited momentum due to small atomic mass is insufficient to overcome the interatomic forces requiring a steep increase in the activation energy to diffuse through the alloy matrix as compared to that in the pure elemental state.

The sluggish diffusion is caused by the presence of a variety of metals in the matrix of the CCA, contributing to several competing strengthening mechanisms. Subsequently, certain superior properties at elevated temperatures [45] are noted, such as excellent creep resistance [21,46]. At $T > 0.5T_m$, deformation by creep becomes significant in addition to time independent yielding. The predominant creep mechanisms *viz.*, dislocation glide creep (at relatively higher stress levels) and the diffusional creep (Nabarro-Herring and Coble creep) are primarily governed by mass diffusion at elevated temperatures. To correlate the sluggish diffusion in CCA with the corresponding creep mechanisms, we consider the Nabarro-Herring strain rate ($\dot{\varepsilon}_{NH}$) [47] and the Coble creep strain rate ($\dot{\varepsilon}_C$) [47].

$$\dot{\varepsilon}_{NH} = A_{NH}\left(\frac{D_L}{d^2}\right)\left(\frac{\sigma\Omega}{kT}\right) \tag{3}$$

$$\dot{\varepsilon}_C = A_C\left(\frac{D_{GB}\delta}{d^3}\right)\left(\frac{\sigma\Omega}{kT}\right) \tag{4}$$

Here, σ is the normal stress, Ω the atomic volume, $D_L$ the lattice diffusion (diffusion through bulk material) coefficient, d the grain size, while $A_{NH}$ and $A_C$ are geometrical parameters, $D_{GB}$ is the grain boundary diffusivity (*a.k.a.* surface diffusivity in case of single crystal), and δ is the grain boundary thickness.

At room temperature grain boundary diffusion is more pronounced than lattice diffusion because of inefficient packing of atoms at grain boundaries. Such an ineffective atomic arrangement results in lower impedance to atom motion relative to the diffusion through the lattice. But at higher temperatures, these diffusion rates converge and can be quantified equally as the bulk diffusion coefficient [48], *i.e.*, $D$. Lowering $D$ by an order of magnitude due to sluggish diffusion will reduce the creep strain rates equivalently per Eqs. (3) and (4). Hence, sluggish diffusion increases the creep resistance of CCAs and augments the span of elastic deformation at elevated temperatures for CCAs. We probe the sluggish diffusion using two parameters *viz.*, $g_{\alpha\text{-}\beta}(r)$ and the $E^x_{MD}$. $g_{\alpha\text{-}\beta}(r)$ can identify neighboring atoms that are (un)favorable for elemental diffusion [27]. As mentioned above, from Fig. S3, we find that the unlike pairs have a strong affinity to coordinate, and hence the inter-element attractive forces dominates the interactions between like atoms, as also noted in the literature [49].

The tendency to form single phase solid-solutions substantiates the existence of strong metallic bonds between the constituent metals and the absence of intermetallic microstructures. As a consequence of such cross interactions, the atomic diffusion is severely constrained within the multi-principle element matrix. Each element experiences a relatively stronger force field in its neighborhood that resists any atomic migration. We support this argument with predictions for the $E^x_{MD}$ of each constituent metal. Note that the LPE before and after the migration of atom to vacancy is same in a matrix that has a like environment in the neighborhood of each atom as in a pure metal. Hence, $E^x_{MD}$ for the five constituent metals in their pure form is zero, as also corroborated by our DFT simulations. But for CCAs where multiple metal atoms coexist in the lattice, $E^x_{MD} \neq 0$. Table 1 lists the corresponding $E^x_{MD}$ for each metallic element in the CCA. $E^x_{MD}$varies from 0.60 eV for Zr to 1.89 eV for migration of a Ta atom to a vacant site. Since each particular atomic configuration in the CCA lattice renders a unique LPE, atoms prefer to arrange themselves in the lowest energy configuration. Such preferential occupancy constrains the atoms from migrating to a vacancy since the atomic reorientation can result in a higher and unstable LPE. Hence the lower energy atomic sites, also referred to as low energy atomic traps

**Table 1**
The mean difference in energies ($E^x_{MD}$) of the Lattice Potential Energy (LPE) for all the metals in $(Mo_{0.95}W_{0.05})_{0.85}Ta_{0.10}(TiZr)_{0.05}$ CCA are listed. Each metal atom is forced to migrate to a vacancy site and the difference in LPE before and after migration is calculated as $E^x_{MD}$. This analysis suggests that in CCAs, there are some preferable sites for each atom type where the resulting LPE is the lowest. Such a preferential element-specific site occupancy creates low energy atomic traps that prevents atoms from migrating to vacancies, and sluggardizing the diffusion by orders of magnitude below that of corresponding pure metals.

| Solute | Mo | Ta | Ti | W | Zr |
|---|---|---|---|---|---|
| $E^x_{MD}$ (eV) | 1.29 | 1.89 | 1.54 | 0.67 | 0.60 |

[20], impede atomic diffusion in CCAs requiring a strong energy barrier to be overcome for such motion. The effect of low energy atomic traps coupled with the strong cross-interactions of the metals in the CCA sluggardize the diffusion in multicomponent alloys.

## 4. Summary

Classical molecular simulations are employed to examine and understand the fundamental causes for the sluggish diffusion of atoms in a representative refractory CCA. The reduced (by a factor of ~8–12) diffusion coefficients of the constituent elements relative to their pure metallic forms, together with higher (~1.5–3 × ) activation energies corroborate the sluggish diffusion effect. We deduce that a two-fold effect causes such poor diffusion, and subsequently an enhanced creep resistance. On one hand, the relatively pronounced attraction between unlike pairs of elements in the CCA than that between like pairs, generates a strong attractive force field in the neighborhood of the atoms that impedes their diffusion by increasing the resistance to atomic movement through higher activation energies; on the other hand, the presence of multiple elemental species in the alloy lattice creates low energy atomic traps. Since the energy barrier associated with the migration of an atom to a vacancy is ~1 eV, such energy penalty inhibits atom movement contributing to a sluggish diffusion. Additionally, we predict that both Nabarro-Herring and Cobble creep deformation strain rates are lowered by an order of magnitude in the CCA relative to that in the corresponding pure metals, supporting the enhanced creep resistance of refractory CCAs at elevated temperatures. The results assist in offering a quantitative reasoning for the sluggish diffusion of the elements in a CCA based on the lattice energies associated with atom migration within the alloy, and activation energies required for atoms to overcome and promote diffusion. The presented computational methodology can be employed for any set of metals and their alloys, and the results can describe the relative changes in their diffusion behaviors when in the alloy compared to when in the pure metal state. This knowledge and data can assist in quantifying the increase in creep resistance of the alloy as recognized by Eqs. (3) and (4), and tuning alloy compositions for targeted applications.

## CRediT authorship contribution statement

**Ankit Roy:** Conceptualization, Methodology, Writing - original draft, Formal analysis, Investigation, Visualization. **Joydeep Munshi:** Investigation. **Ganesh Balasubramanian:** Writing - review & editing, Supervision, Project administration, Funding acquisition.

## Declaration of competing interest

The authors declare that they have no known competing financial interests or personal relationships that could have appeared to influence the work reported in this paper.

## Acknowledgements

The research was supported, in part, by the National Science Foundation (NSF) through the award CMMI-1944040, and the Ames Laboratory through the U.S. Department of Energy (DOE), Office of Energy Efficiency and Renewable Energy, Advanced Manufacturing Office (AMO) under design project WBS 2.1.0.19. Ames Laboratory is operated by Iowa State University for the U.S. DOE under contract DE-AC02-07CH11358.

## Appendix A. Supplementary data

Supplementary data to this article can be found online at https://doi.org/10.1016/j.intermet.2021.107106.

## Data availability

The data and methods reported in this paper are available from the corresponding author upon reasonable request.

## References

[1] J.-W. Yeh, S.-J. Lin, T.-S. Chin, J.-Y. Gan, S.-K. Chen, T.-T. Shun, C.-H. Tsau, S.-Y. Chou, Formation of simple crystal structures in Cu-Co-Ni-Cr-Al-Fe-Ti-V alloys with multiprincipal metallic elements, Metall. Mater. Trans. 35 (8) (2004) 2533–2536.
[2] B. Cantor, I. Chang, P. Knight, A. Vincent, Microstructural development in equiatomic multicomponent alloys, Mater. Sci. Eng. A 375 (2004) 213–218.
[3] O. Senkov, G. Wilks, D. Miracle, C. Chuang, P. Liaw, Refractory high-entropy alloys, Intermetallics 18 (9) (2010) 1758–1765.
[4] O.N. Senkov, D.B. Miracle, K.J. Chaput, J.-P. Couzinie, Development and exploration of refractory high entropy alloys—a review, J. Mater. Res. 33 (19) (2018) 3092–3128.
[5] O.N. Senkov, G.B. Wilks, J.M. Scott, D.B. Miracle, Mechanical properties of Nb25Mo25Ta25W25 and V20Nb20Mo20Ta20W20 refractory high entropy alloys, Intermetallics 19 (5) (2011) 698–706.
[6] J.M. Rickman, H.M. Chan, M.P. Harmer, J.A. Smeltzer, C.J. Marvel, A. Roy, G. Balasubramanian, Materials informatics for the screening of multi-principal elements and high-entropy alloys, Nat. Commun. 10 (1) (2019) 2618.
[7] A. Roy, T. Babuska, B. Krick, G. Balasubramanian, Machine learned feature identification for predicting phase and Young's modulus of low-, medium-and high-entropy alloys, Scripta Mater. 185 (2020) 152–158.
[8] M.-H. Chuang, M.-H. Tsai, W.-R. Wang, S.-J. Lin, J.-W. Yeh, Microstructure and wear behavior of AlxCo1. 5CrFeNi1. 5Tiy high-entropy alloys, Acta Mater. 59 (16) (2011) 6308–6317.
[9] E. Osei-Agyemang, G. Balasubramanian, Surface oxidation mechanism of a refractory high-entropy alloy, NPJ Mater. Degradation 3 (1) (2019) 20.
[10] C.-Y. Hsu, C.-C. Juan, W.-R. Wang, T.-S. Sheu, J.-W. Yeh, S.-K. Chen, On the superior hot hardness and softening resistance of AlCoCrxFeMo0. 5Ni high-entropy alloys, Mater. Sci. Eng. A 528 (10–11) (2011) 3581–3588.
[11] B. Gwalani, R. Salloom, T. Alam, S. Valentin, X. Zhou, G. Thompson, S. Srinivasan, R. Banerjee, Composition-dependent apparent activation-energy and sluggish grain-growth in high entropy alloys, Mater. Res. Lett. 7 (7) (2019) 267–274.
[12] M. Vaidya, K. Pradeep, B. Murty, G. Wilde, S. Divinski, Bulk tracer diffusion in CoCrFeNi and CoCrFeMnNi high entropy alloys, Acta Mater. 146 (2018) 211–224.
[13] Y. Zhang, T.T. Zuo, Z. Tang, M.C. Gao, K.A. Dahmen, P.K. Liaw, Z.P. Lu, Microstructures and properties of high-entropy alloys, Prog. Mater. Sci. 61 (2014) 1–93.
[14] M.-H. Tsai, J.-W. Yeh, J.-Y. Gan, Diffusion barrier properties of AlMoNbSiTaTiVZr high-entropy alloy layer between copper and silicon, Thin Solid Films 516 (16) (2008) 5527–5530.
[15] P. Gopal, S. Srinivasan, First-principles study of self-and solute diffusion mechanisms in γ′-Ni 3 Al, Phys. Rev. B 86 (1) (2012), 014112.
[16] B.S. Murty, J.-W. Yeh, S. Ranganathan, P. Bhattacharjee, High-entropy Alloys, Elsevier2019.
[17] M.C. Gao, D.E. Alman, Searching for next single-phase high-entropy alloy compositions, Entropy 15 (10) (2013) 4504–4519.
[18] M. Rappaz, W. Boettinger, On dendritic solidification of multicomponent alloys with unequal liquid diffusion coefficients, Acta Mater. 47 (11) (1999) 3205–3219.
[19] G.H. Vineyard, Theory of order-disorder kinetics, Phys. Rev. 102 (4) (1956) 981.
[20] K.-Y. Tsai, M.-H. Tsai, J.-W. Yeh, Sluggish diffusion in Co–Cr–Fe–Mn–Ni high-entropy alloys, Acta Mater. 61 (13) (2013) 4887–4897.
[21] P. Singh, A. Sharma, A.V. Smirnov, M.S. Diallo, P.K. Ray, G. Balasubramanian, D. D. Johnson, Design of high-strength refractory complex solid-solution alloys, NPJ Comput. Mater. 4 (1) (2018) 16.
[22] D. Beke, G. Erdélyi, On the diffusion in high-entropy alloys, Mater. Lett. 164 (2016) 111–113.
[23] S. Plimpton, Fast Parallel Algorithms for Short-Range Molecular Dynamics, Sandia National Labs., Albuquerque, NM (United States), 1993.

[24] K. Momma, F. Izumi, VESTA 3 for three-dimensional visualization of crystal, volumetric and morphology data, J. Appl. Crystallogr. 44 (6) (2011) 1272–1276.
[25] A. Stukowski, Visualization and analysis of atomistic simulation data with OVITO–the Open Visualization Tool, Model. Simulat. Mater. Sci. Eng. 18 (1) (2009), 015012.
[26] X. Zhou, R. Johnson, H. Wadley, Misfit-energy-increasing dislocations in vapor-deposited CoFe/NiFe multilayers, Phys. Rev. B 69 (14) (2004), 144113.
[27] A. Sharma, P. Singh, D.D. Johnson, P.K. Liaw, G. Balasubramanian, Atomistic clustering-ordering and high-strain deformation of an Al 0.1 CrCoFeNi high-entropy alloy, Sci. Rep. 6 (2016) 31028.
[28] J. Yuan-Yuan, Z. Qing-Ming, G. Zi-Zheng, J. Guang-Fu, Molecular dynamics simulation of self-diffusion coefficients for liquid metals, Chin. Phys. B 22 (8) (2013), 083101.
[29] M.P. Allen, D.J. Tildesley, Computer Simulation of Liquids, Oxford university press2017.
[30] R. LeSar, Introduction to Computational Materials Science: Fundamentals to Applications, Cambridge University Press2013.
[31] J. Hafner, Ab-initio simulations of materials using VASP: density-functional theory and beyond, J. Comput. Chem. 29 (13) (2008) 2044–2078.
[32] W. Chen, X. Ding, Y. Feng, X. Liu, K. Liu, Z. Lu, D. Li, Y. Li, C. Liu, X.-Q. Chen, Vacancy formation enthalpies of high-entropy FeCoCrNi alloy via first-principles calculations and possible implications to its superior radiation tolerance, J. Mater. Sci. Technol. 34 (2) (2018) 355–364.
[33] G. Kresse, D. Joubert, From ultrasoft pseudopotentials to the projector augmented-wave method, Phys. Rev. b 59 (3) (1999) 1758.
[34] P.E. Blöchl, Projector augmented-wave method, Phys. Rev. B 50 (24) (1994) 17953.
[35] J.P. Perdew, K. Burke, M. Ernzerhof, Generalized gradient approximation made simple, Phys. Rev. Lett. 77 (18) (1996) 3865.
[36] Y. Qi, T. Çağın, Y. Kimura, W.A. Goddard III, Molecular-dynamics simulations of glass formation and crystallization in binary liquid metals: Cu-Ag and Cu-Ni, Phys. Rev. B 59 (5) (1999) 3527.
[37] Y. Tong, S. Zhao, H. Bei, T. Egami, Y. Zhang, F. Zhang, Anomalous Local Distortion in BCC Refractory High-Entropy Alloys, 2019 arXiv preprint arXiv:1902.09279.
[38] N.W. Ashcroft, N.D. Mermin, Solid State Physics [by] Neil W. Ashcroft [and] N. David Mermin, Holt, Rinehart and Winston, New York, 1976.
[39] M. Ghafari, H. Gleiter, T. Feng, H. Hahn, Are transition metal-rich metallic glasses made up of distorted BCC clusters, J. Mater. Sci. Eng. 5 (2016), 1000299-1.
[40] H.J. Frost, M.F. Ashby, Deformation Mechanism Maps: the Plasticity and Creep of Metals and Ceramics, Pergamon press, 1982.
[41] Z. Cui, X. Zhou, Q. Meng, Atomic-scale mechanism investigation of mass transfer in laser fabrication process of Ti-Al alloy via molecular dynamics simulation, Metals 10 (12) (2020) 1660.
[42] J. Ding, M. Asta, R.O. Ritchie, Melts of CrCoNi-based high-entropy alloys: atomic diffusion and electronic/atomic structure from ab initio simulation, Appl. Phys. Lett. 113 (11) (2018), 111902.
[43] D. Beke, I. Gödény, F. Kedves, G. Erdélyi, Connections between thermodynamic quantities and vacancy and diffusion characteristics in binary metallic solid solutions, J. Phys. Chem. Solid. 40 (7) (1979) 543–555.
[44] D.L. Beke, Tracer Diffusion in Homogeneous and Heterogeneous Alloys, Defect and Diffusion Forum, Trans Tech Publ, 1992, pp. 31–54.
[45] Z. Wu, H. Bei, G.M. Pharr, E.P. George, Temperature dependence of the mechanical properties of equiatomic solid solution alloys with face-centered cubic crystal structures, Acta Mater. 81 (2014) 428–441.
[46] T.-K. Tsao, A.-C. Yeh, C.-M. Kuo, K. Kakehi, H. Murakami, J.-W. Yeh, S.-R. Jian, The high temperature tensile and creep behaviors of high entropy superalloy, Sci. Rep. 7 (1) (2017) 1–9.
[47] T.H. Courtney, Mechanical Behavior of Materials, Waveland Press2005.
[48] A.R. Wazzan, Lattice and grain boundary self-diffusion in nickel, J. Appl. Phys. 36 (11) (1965) 3596–3599.
[49] W.P. Huhn, M. Widom, Prediction of A2 to B2 phase transition in the high-entropy alloy Mo-Nb-Ta-W, JOM (J. Occup. Med.) 65 (12) (2013) 1772–1779.